Comparison of the Heat Transfer Capabilities of Conventional Single- and Two-Phase Cooling Systems for an Electric Vehicle IGBT Power Module

Itxaso Aranzabal, Iñigo Martínez de Alegría, Nicola Delmonte, *Member, IEEE*, Paolo Cova, and Iñigo Kortabarria

***Abstract*—This paper presents a comparison of conventional single-phase water/glycol liquid and innovative two-phase cooling technology for thermal management of high-power electronics automotive insulated-gate bipolar transistor modules during a full drive cycle. The proposed two-phase cooling system is built using conventional automotive air conditioning components (a condenser, an expansion valve, a compressor, and vapor and liquid lines) and a conventional cold plate as used for single-phase cooling; thus, the design does not require the development of new technology for its implementation. Three-dimensional numerical simulation in COMSOL and experimental results of two-phase cooling have been obtained on a prototype and compared to conventional water/glycol cooling high-power electronics modules, with a considerable improvement on working temperature, power transfer capacity, and equalization of die temperatures during a full driving cycle. These results suggest that two-phase cooling using the same cold plates as in single-phase cooling can be used to substantially improve the performance and reliability of electric vehicle power converters without major changes.**

***Index Terms*—Electronics cooling, power electronics, thermal management, thermal resistance.**

I. Introduction

High-power-density electric vehicle (EV) power inverters require a new approach to cope with stringent requirements of high current density, excessive ambient temperatures, humidity, vibrations, dirt in the engine compartment, reliability, and cost. The heat flux of power insulated-gate bipolar transistor (IGBT) modules for EVs is in the range of 100–150 W/cm^2, and it is projected to increase to 500 W/cm^2, as the current densities and switching frequencies increase [1]–[3]. The development of new die technologies, such as wide bandgap (WBG), requires innovative cooling methods to achieve an efficient implementation [4]. Silicon die power dissipation is close to 100 W/cm^2, while WBG dies can reach up to 1 kW/cm^2, so new efficient cooling technologies are necessary [4].

Manuscript received January 22, 2018; revised May 15, 2018; accepted July 26, 2018. Date of publication August 2, 2018; date of current version March 29, 2019. This work was carried out at the Research and Education Unit UFI11/16 of the University of the Basque Country (UPV/EHU) and supported in part by the Department of Education, Linguistic Policy and Culture of the Basque Government under the fund for research groups of the Basque University System IT978-16, in part by the Ministerio de Economía y Competitividad of Spain under Project DPI2014-53685-C2-2-R and FEDER funds, and in part by the Government of the Basque Country under the research program ELKARTEK as the Project KT4TRANS (KK-2015/00047 and KK-2016/00061). Recommended for publication by Associate Editor J. Wang. *(Corresponding author: Itxaso Aranzabal.)*

I. Aranzabal, I. Martinez de Alegria, and I. Kortabarria are with the Universidad del País Vasco/Euskal Herriko Unibertsitatea (University of the Basque Country), 48940 Bilbao, Spain (e-mail:

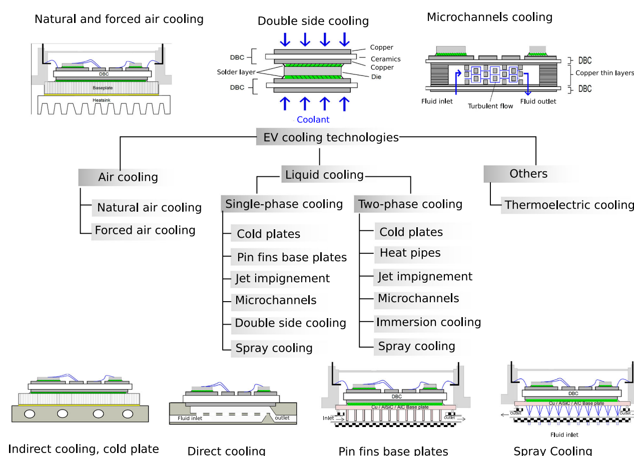

Fig. 1. Classification of EV power module cooling technologies.

Power semiconductor devices may incur failures and lifetime reduction if the maximum junction temperature given by the manufacturer is exceeded [5], [6] and when the power cycling produces a high temperature swing [7]. Therefore, a prediction of the chip temperature in the design process is crucial for a reliable IGBT module thermal design, as well as the heat sink design, which affects the total converter size, weight, and cost. The reliability of power electronic systems is also closely dependent on the thermal behavior of semiconductor devices. In [8], it is demonstrated that, for a 1.7-kV IGBT technology power inverter, increasing the cooling capacity from 50 to 120 W/cm^2, the current density increases from 40 to 80 A/cm^2.

Many technologies and techniques for cooling EV power modules can be found in the literature, as shown in Fig. 1 [1], [5], [9]–[31]. In [32], a review and classification of the main thermal management techniques is presented.

In two-phase cooling systems, the boiling effect provides the possibility of increasing heat absorption per unit volume of

See http://www.ieee.org/publications_standards/publications/rights/index.html for more information.

fluid and higher heat acquisition effectiveness (i.e., the amount of heat absorbed by a unit of flow relative to its maximum theoretical capacity). This latent heat benefit is coupled with the improved convection due to buoyancy-driven bubble formation, multiphase turbulation, and mixing that takes place within the heat transfer region. In this way, the resultant heat transfer coefficients from two-phase flow can be an order of magnitude greater than equivalent single-phase forced convection. A larger heat transfer coefficient translates directly into a larger cooling capacity for the system [33], allowing lower flow rates and lower pumping power than the conventional single-phase water/glycol cold plates. In spite of these advantages, the unconventional design tradeoffs in two-phase cold plates have limited the introduction of two-phase cooling in automotive power inverters.

Several papers in the scientific literature present results on two-phase cooling techniques for the removal of high heat flux. In [14] and [34], the authors designed a pump vaporizable dielectric fluid cooling system for power electronics systems; in [35]–[37], the authors designed a two-phase microchannel heat sink capable of obtaining a heat transfer coefficient up to 50 000 $\mathrm{W/m^2 \cdot K}$. In [38], thermal simulation is used to study the effect of the convective heat transfer coefficient, cold plate dimensions, and total power dissipated by IGBTs on the thermal performance of the power module.

A few authors present a two-phase cooling system based on conventional air conditioning (A/C) components. The Oak Ridge National Laboratory designed a two-phase cooling floating loop based on the EV passenger compartment A/C refrigerant system [39], [40]. In [41], a passive two-phase cooling has been designed for automotive power electronics. In [42], a device-level analytical modeling and system-level thermal simulation is used to examine and compare single-phase and two-phase cold plates for an inverter module. However, no direct experimental data are available for comparison of single- and two-phase cooling of the EV power inverter working through the same full drive cycle, in order to assess both systems.

This paper is focused on improving the reliability of EV power converters using a two-phase cooling system with a cold plate and R134-a coolant. R134-a is already available in an automotive A/C system; it is environment friendly and has good heat transfer and dielectric properties [14], [43], [44].

The main goal of this work is to test and compare an experimental vapor compression two-phase loop (VCTPL) prototype built using conventional automotive A/C components (a condenser, an expansion valve, a compressor, and vapor and liquid lines) with a conventional single-phase cooling system under the same drive cycle.

Because the heat transfer coefficient h is not a parameter provided by manufacturers of cold plates for conventional single-phase cooling, it is necessary to determine experimentally the value of h for a specific cold plate (NHC-152), before detailed three-dimensional (3-D) finite-element method (FEM) simulation of the two-phase cooling of IGBTs in the motor inverter could be done. Single- and two-phase cooling on the same cold plate has been numerically compared with multiphysics simulations to address the advantages of the first solution from the point of view of the conversion efficiency and the system reliability.

The following sections are presented:

1) an experimental determination of the heat transfer coefficient, h, of the NHC-152 cold plate for SKIM power modules;
2) the experimental results of single- and two-phase cooling under a full drive cycle;
3) a 3-D thermal simulation under steady-state conditions of single- and two-phase cooling using the same cold plate.

II. Experimental Characterization

By thermal characterization of the cold plate operating in single- and two-phase modes, it has been possible to evaluate the thermal resistance and the heat transfer coefficient of the module operating at different conditions.

Before the cold plate characterization results are presented, the test benches will be discussed.

A. Two-Phase Cooling System Experimental Platform Description

A VCTPL technology has been developed based on the conventional vapor compression refrigeration technique. The prototype consists of the following:

1) an evaporator (the power module cold plate is incorporated as evaporator in VCTPL);
2) a condenser to transfer the heat load to ambient air;
3) a compressor designed to use with dielectric fluids;
4) an electronic expansion valve;
5) ancillary components, for system design specifications, which include a filter, pressure transducers, manometers, and thermocouples.

A schematic diagram of a VCTPL is shown in Fig. 2(a), illustrating its different parts and the fluid direction inside it. Fig. 2(b) shows a picture of the experimental platform.

Under steady-state conditions, when the heat released from the power module is transferred to the cold plate, the liquid starts to vaporize (R134-a refrigerant vaporizes at a low T_{sat} temperature) and absorbs the heat from the power module. In the test bench of Fig. 2(b), to easily generate a controlled heat, three power resistors in series have been used, instead of a semiconductor power module.[1]

The vapor passes through the compressor, where it is brought to high pressure, at a temperature typically 10–15 °C higher than ambient. This hot vapor is converted to liquid in the condensing heat exchanger, where heat is transferred to the ambient air. The hot liquid refrigerant then exits the condenser and passes through an expansion valve, dropping the refrigerant to a low pressure and temperature. The low-temperature low-pressure liquid refrigerant then enters the evaporator, and the cycle begins again.

An electronic valve and a proportional–integral controller are used to ensure that the compressor is always fed with superheated gas, and it is not damaged. In order to ensure that the

[1] In order to reduce the heat transferred to the air and ensure that the dissipated power is equal to the heat absorbed by the cold plate, the evaporator system has been thermally isolated by styrofoam material.

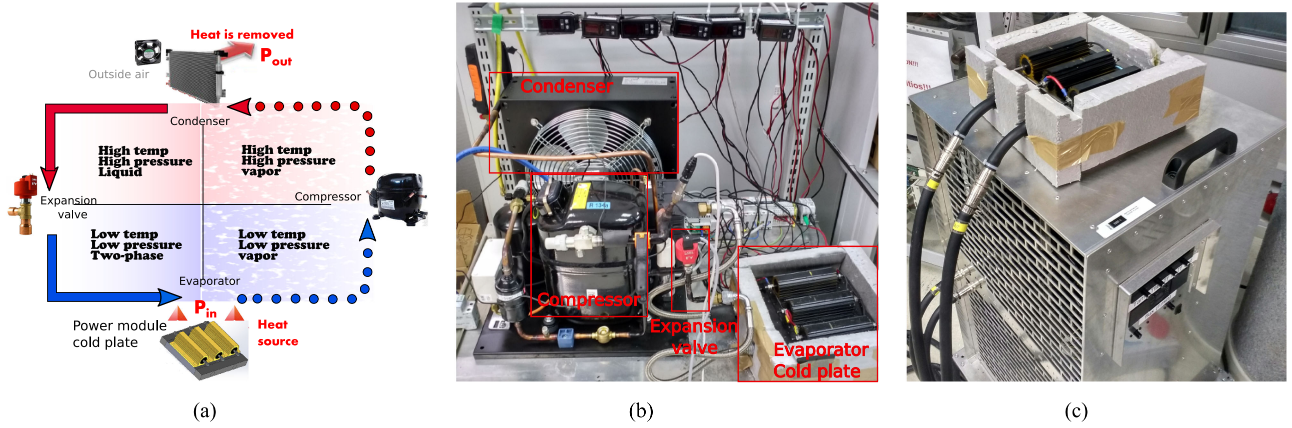

(a) (b) (c)

Fig. 2. Developed experimental platforms of EV power module cooling systems. (a) Schematic diagram of the experimental vapor compression loop. (b) Experimental vapor compression loop. (c) Experimental water/glycol cooling system.

critical heat flux, where bubbles are too big and dry out may occur, is not reached, the system is monitored in order to detect very sudden temperature increase. However, during tests, the critical heat flux was never reached.

Vapor compression systems take advantage of the liquid latent heat vaporization that has a boiling point lower than the desired temperature to be managed.

B. Single-Phase Cooling System Description

In order to provide a baseline for comparison, the performance of the power inverter module with single-phase convective cooling has been included. In this way, for the single-phase cooling, a water/glycol LCS-W2x420PRO liquid cooling system has been used [see Fig. 2(c)]. The main elements are the following:

1) two pumps to circulate the water in the closed cooling loop;
2) 36 air fans to transfer the heat to the air;
3) fan speed controller: it regulates the fan speed depending on the fluid outlet temperature;
4) ancillary components, for system design specifications, which include a filter, thermocouples, a flow meter, and pump regulators.

The low-temperature water/glycol flow generated by the recirculating pump goes to the cold plate, which absorbs the heat generated by the power module mounted on it. The hot liquid at the outlet of the cold plate is cooled by 36 fans located along the cooling loop, and the heat is transferred to ambient air. Fan speed is controlled as a function of the fluid outlet temperature.

C. Experimental Determination of the Cold Plate Heat Transfer Coefficient, h

To characterize the cold plate and evaluate its performance, it is necessary to analyze the value of the thermal resistance $R_{(s-f)}$. In a first approximation, in order to emulate the thermal pattern of a high-density power module, following the procedure described in [45], the cold plate is heated by the Joule effect using three series-connected 22-Ω 300-W power resistors, with a capacity to dissipate up to a maximum power of 900 W. For steady-state conditions, the temperatures measured on the cold plate have variations less than a tenth of a degree over a period of about 20 min.

The manufacturer of the NHC-152 cold plate provides a nominal thermal resistance, $R_{\text{th}(s-f)}$, of 0.016 K/W for single-phase liquid cooling. However, for the two-phase cooling system, due to the simultaneous existence of the two phases and possible thermal transport by convection and boiling, predicting this value is very challenging. In order to obtain accurate numerical models, a correct value of h is necessary.

When the thermophysical properties (i.e., vapor quality, pressure inside the cold plate, flow rate, etc.) in the evaporation process are unknown, based on previous studies [37], [46]–[48], the expression used to determine the average heat transfer coefficient h is the following:

$$h = \frac{1}{R_{(w-f)} \cdot A} \tag{1}$$

$$R_{(w-f)} = R_{(s-f)} - R_{(s-w)} \tag{2}$$

$$R_{(s-f)} = \frac{Ts_{\text{avg}} - T_f}{P_d} \tag{3}$$

$$T_f = \frac{T_{\text{out}} + T_{\text{in}}}{2} \tag{4}$$

$$R_{(s-w)} = \frac{d_m}{\lambda \cdot A} \tag{5}$$

where $R_{(w-f)}$ is the thermal resistance from the cold plate internal channel wall to the fluid, $R_{(s-f)}$ is the total thermal resistance from the cold plate to the fluid, $R_{(s-w)}$ is the thermal resistance from the cold plate top surface to the internal channel wall obtained by conduction, Ts_{avg} is the average temperature of the cold plate surface,[2] T_f is the average fluid temperature, T_{in} is the saturation temperature of the refrigerant in the test section, which is measured by a temperature probe located at the inlet of the evaporator, T_{out} is the overheating saturation temperature of the refrigerant in the test section, which is measured by a

[2] Ts_{avg} was directly measured by thermocouples placed on the cold plate surface and contrasted by thermograms taken by an IR camera FLIR SC 430.

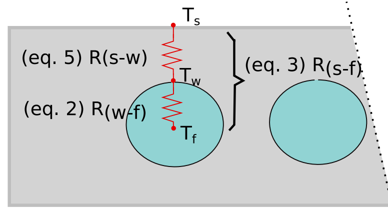

Fig. 3. Thermal resistance network of the cold plate.

TABLE I
COLD PLATE CHARACTERIZATION FOR SINGLE- AND TWO-PHASE COOLING TECHNOLOGY

Pd (W)	**Technology**	T_f (°C)	Ts_{avg} (°C)	**h** (W/m^2K)	R_{s-f} (K/W)
340	Single-phase	25.5	31.2	1362	0.016
340	Two-phase	-11.25	-6.5	1581	0.015
460	Single-phase	25.5	33.25	1344	0.016
460	Two-phase	-9	-3.2	1958	0.013
600	Single-phase	25.5	34.25	1535	0.015
600	Two-phase	-6.7	0.15	2213	0.011
760	Single-phase	27	37.05	1730	0.013
760	Two-phase	-6.65	0.9	2517	0.009
945	Single-phase	27	39.5	1862	0.013
945	Two-phase	-6.65	1.49	2953	0.008

temperature probe located at the outlet of the evaporator, λ is the cold plate material thermal conductivity, d_m is the distance from the cold plate top surface to the internal channel wall, P_d is the power dissipated in the module (or the total heat absorbed by the cold plate), and A is the cold plate top surface heat transfer area. Fig. 3 shows the physical meaning of all the terms.

Table I presents $R_{(s-f)}$ for single-phase cooling and h and $R_{(s-f)}$ for two-phase cooling.

These experimental results are in accordance with data provided by cold plate's manufacturer. The results demonstrate that an R134a-cooled two-phase cooling system at a flow rate of 0.2 L/min can reach values for the heat transfer coefficient and the thermal resistance around 1500 and 3000 $W/m^2 \cdot K$, and 0.008 and 0.015 K/W, respectively.

The results demonstrate that for the R134a-cooled two-phase cooling system, when the heat flux is increased, the flow boiling heat transfer coefficient increases, which is an indication of the nucleate boiling regime [49].

Fig. 4 shows the average temperature measured on the resistor top surface for different dissipate powers operating in single- and two-phase cooling modes.

III. WORLDWIDE HARMONIZED LIGHT VEHICLES TEST PROCEDURE (WLTP) DRIVING CYCLE THERMAL RESPONSE

In this section, a comparison of single- and two-phase cooling when a WLTP driving cycle is applied to the load is shown. Additionally, to test the performance of the cooling system under close to real EV drive operation conditions, a loss versus time curve [see Fig. 5(a)] derived from a WLTP driving cycle [50] has been applied to the load. Driving cycles are standardized series of points, determined by governments or organizations, that represent the speed profile of a given vehicle versus time [51]. The target of driving cycles is to estimate the CO_2 emissions, energy consumption, and autonomy of the vehicles. Torque, mechanical power, and power losses depend on the drive and vehicle characteristics. In this particular case, inverter losses have been estimated considering a 64-kW drive of a B-segment EV.

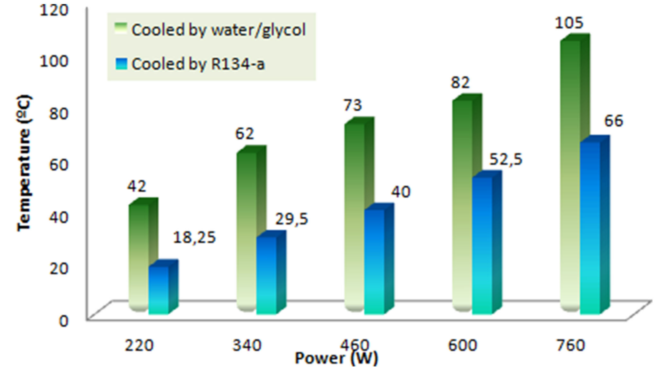

Fig. 4. Resistor surface maximum temperature operating in single- and two-phase cooling modes.

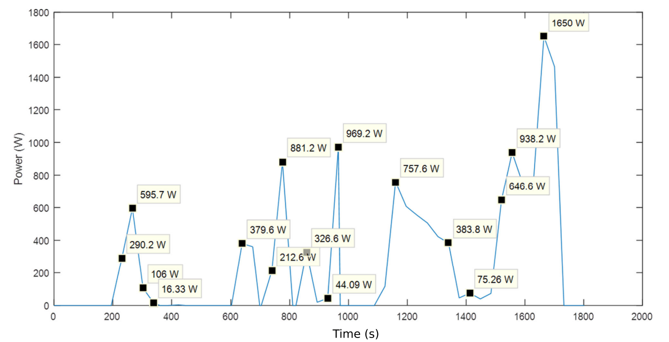

(a)

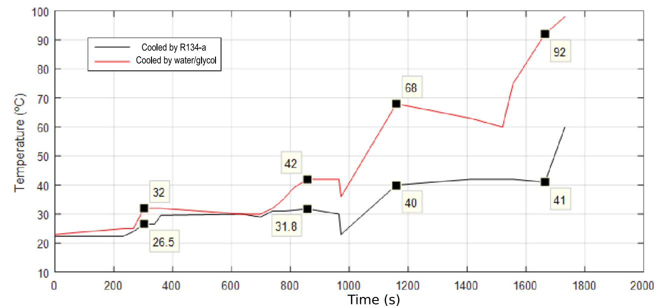

(b)

Fig. 5. Maximum resistor surface temperature obtained experimentally when a WLTP driving cycle is applied to the load. (a) Loss versus time curve derived from a WLTP driving cycle. (b) Maximum resistor top surface temperature.

The results of the experiment demonstrate that for an R134a-cooled two-phase cooling system, the maximum resistor top surface temperatures are kept below the temperatures obtained in a water/glycol cooled system under same operation conditions. Therefore, two-phase cooling offers the possibility to run the module at higher current density and realize the same power

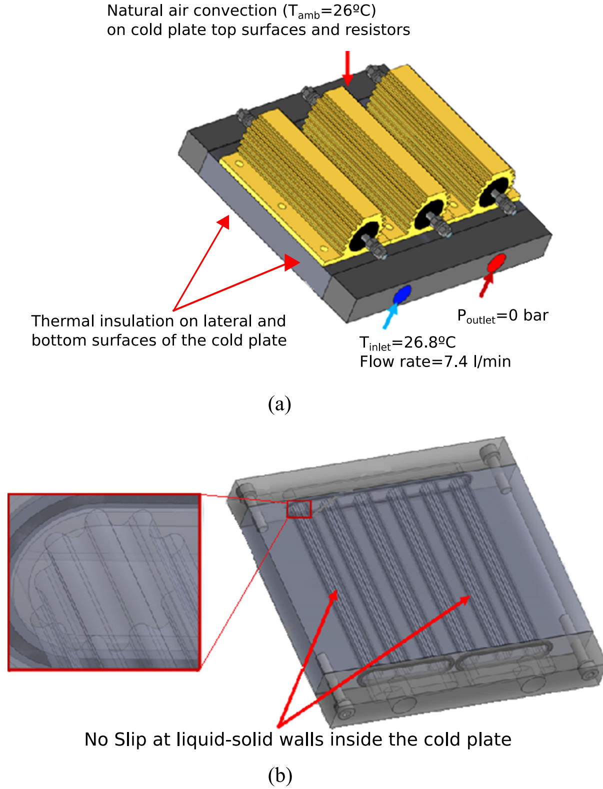

Fig. 6. (a) Three-dimensional geometry of the single-phase numerical model with external boundary conditions of the thermal-fluid dynamic problem. (b) Three-dimensional geometry of the cold plate with inner boundary conditions for computational fluid dynamic.

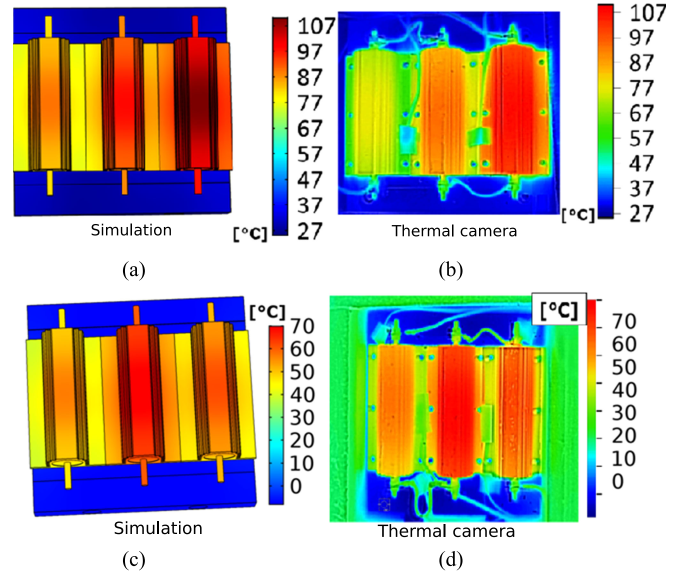

Fig. 7. Thermal maps resulting by a simulation at steady state with a total dissipated power of 700 W. (a) Single-phase cooling; P_d of 700 W, flow rate $= 7.4$ L/min, $T_{\text{inlet}} = 27$ °C, and $T_{\text{amb}} = 26$ °C. (b) Two-phase cooling; P_d of 700 W, flow rate $= 0.2$ L/min, and $T_{\text{sat}} = -8$ °C.

level with fewer devices and smaller/lighter weight packaging, resulting in significant potential cost savings.

IV. Numerical Modeling

This section describes 3-D simulations using COMSOL Multiphysics of single- and two-phase cooling using an NHC-152 cold plate for an SKIM909GD066 inverter.

A. Geometry and Boundary Conditions for 3-D Simulation

Fig. 6(a) shows the 3-D geometry of the cold plate with the power resistors used during the experimental characterization with the boundary conditions set in the numerical model. The dissipated power is distributed uniformly along the wounded resistance. The cold plate shown in Fig. 6(b) is composed by two three-column thermosiphons in series. The column section is circular with fins.

With COMSOL Multiphysics, while a fully coupled thermal-fluid dynamic single-phase problem can be modeled with no particular troubles, the same problem with the two-phase cooling cannot be easily set. The main problem in the last case is to couple the heat transfer in solids with the evaporation of the coolant in the cold plate.

The experimental characterization described in Section II has been made to:

1) validate the thermal-fluid dynamic models of the single-phase cooling;
2) evaluate the thermal resistance of the cold plate when used for the two-phase cooling, in order to avoid the simulation of the evaporation, which requires a complex model with two-phase change (liquid to gas) and vapor saturation.

Simulation of the complex two-phase phenomenon, with thermal transport by boiling and convection, has been simplified with a good matching between simulation and experimental results by the substitution of all the mechanisms by a simple uniform heat transfer coefficient, h, along the inner walls of the cold plate.

B. Single-Phase Modeling Validation

The water–propylene glycol 40% mixture, with a no-slip boundary condition (the fluid will have zero velocity relative to the boundary) at the surfaces in contact with the aluminum cold plate channel wall, has been set as a coolant.

Steady-state simulations for different dissipated power levels in the resistors have been obtained and compared with experimental results using thermogram images obtained using a FLIR SC 430 thermal camera.

The matching between simulations and experimental is good as can be seen comparing the thermal maps shown in Fig. 7(a).

In this model, the uncertainty arises mainly by the thermal contact resistance (TCR) between the resistors and the cold plate because these parts are not clamped with well-known strength. Thus, even if the thermal resistance of the Silpad used as a thermal filler is known, the TCR set in the model was used as a fitting parameter.

C. Two-Phase Modeling Validation

As stated above for this case, the two-phase fluid mechanics and heat transfer details were simplified using the estimated heat

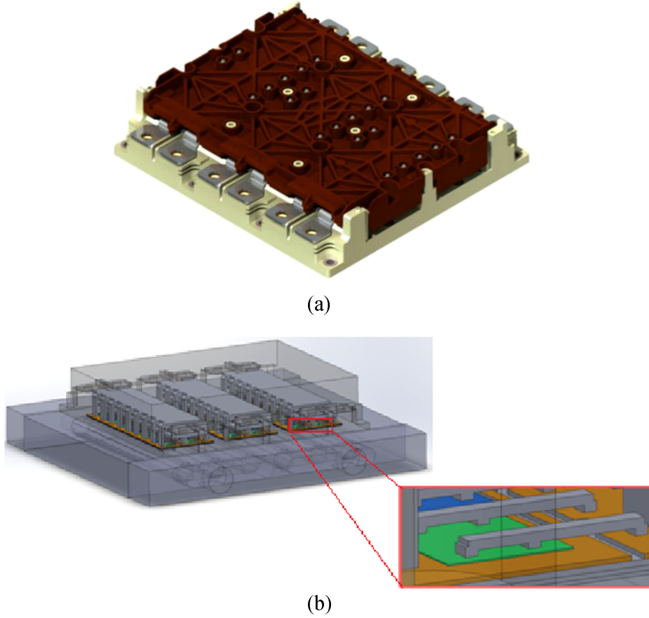

Fig. 8. (a) SKIM909GD066 power module: view of the package. (b) Transparency of the SKIM909GD066 module mounted on the cold plate adopted in this work. The zoomed-up inset shows how the thermal bridges are modeled by replacing the bonding wires.

TABLE II
IGBT POWER MODULE PACKAGE MATERIAL PROPERTIES

Sheet	Materials	Thickness mm	Ther. conduct. $W/m \cdot K$	Spec. heat $J/kg \cdot K$	Density kg/m^3
IGBT chip	Silicon	0.15	130	700	2329
FWD chip	Silicon	0.24	130	700	2329
Die-attach	Ag sinter	0.02	250	230	7350
DBC copper 1	Copper	0.30	400	385	8960
Ceramic	Al_2O_3	0.38	35	730	3965
DBC copper 2	Copper	0.30	400	385	8960
TIM	TIM	0.25	2	1000	2900

transfer coefficient, h, at the inner walls and setting a constant border condition all along the walls of the inner tubes of the cold plate. Fig. 7(b) shows the thermal maps obtained by simulation and measurement in the case of $P_d = 700$ W, $h = 2600$ W/m$^2 \cdot$ K, and $T_{\text{sat}} = -8$ °C.

The large difference observed in the temperature values and in temperature distribution [see Fig. 7(a) and (b)] is due to the different physics governing both cooling solutions, where the capacity of heat absorption through the phase change is much higher than through single-phase convection.

D. Numerical Analysis With a SKIM909GD066 Power Module

The SKIM909GD066 module has been especially designed for automotive applications with high power densities and harsh environmental condition operation capabilities [52]. The package and the layout at the silicon devices level are shown in Fig. 8(a). Table II shows the thermal properties of each layer.

The main goal of this section is to present the comparison of die temperatures in the SKIM module between both single- and two-phase cooling techniques.

The device temperature depends on the internal package thermal resistance, which is introduced in COMSOL using an accurate model with a detailed 3-D geometry of all the layers of the SKIM module and the thermal resistance of the cooler. The thermal resistances of the cooler for single- and two-phase cooling are those obtained in the previous sections, based on the experimentally obtained heat transfer coefficient, h. The uncertainty on the simulation results is reduced to acceptable levels, with an estimated maximum error of around $\pm 5\%$ [45].

This methodology simplifies the simulation process avoiding the time-consuming cosimulation of heat transfer and fluid dynamics modules in COMSOL. After a valid equivalent heat transfer coefficient, h, has been obtained for the two-phase cooled cold plate, only the COMSOL heat transfer module is necessary in order to compare solutions and to evaluate the heat spreading and thermal crosstalk among IGBTs and diodes of the power model and, in turn, to evaluate the temperature of the silicon devices of the module.

The cold plate has been modeled as done for the cases described in Sections IV-B and IV-C. In order to keep the degrees of freedom as low as possible, the geometry of the module has been simplified, as shown in Fig. 8(b), drawing the top cover flat and replacing the bonding wires with geometrically simpler equivalent thermal bridges. After performing distinct simulations to observe the effect of the thermal gel (commonly used to fill the space between the plastic top cover and the power modules), it has been concluded that the utilization of thermal gel barely affects the results because almost all the heat flows toward the cold plate. Thus, to further simplify the model, the power modules were considered as encapsulated in a homogeneous plastic top cover. The simulations were carried out to solve steady-state operating conditions, setting the power dissipated by each IGBT and diode of the power module, considering the heat generated by a diode, the half of the one generated by an IGBT. The simulation results are shown in the next section.

V. RESULTS AND DISCUSSION

This section analyzes the results obtained in the FEM simulations using two different approaches: single-phase cooling, using water as the coolant, and two-phase cooling, using R-134a as the coolant.

A. Comparison of Single- and Two-Phase Results

By the FEM analysis, it was found that an R134a-cooled two-phase cold plate can achieve a much lower device junction temperature at a much lower mass flow rate than a water-cooled single-phase cold plate. In this sense, thermal simulations of the power inverter show that two-phase cooling can provide much better IGBT cooling performance at a lower flow rate [see Tables III and IV, where the IGBTs were numbered, as shown in Fig. 9(a)]. For example, in the case of a dissipated power of

TABLE III
SIMULATED SKIM909GD066 IGBT MAXIMUM JUNCTION TEMPERATURES (IN °C) USING AN R134-A TWO-PHASE COOLING SYSTEM WITH $T_{SAT} = -8$ °C, FLOW RATE = 0.2 L/min, AND $P_d = 2106$ W (52 W/IGBT, 13 W/DIODE)

IGBT1	IGBT1	IGBT2	IGBT3	IGBT4	IGBT5	IGBT6	IGBT7	IGBT8	IGBT9	IGBT10	IGBT11	IGBT12	IGBT13	IGBT14	IGBT15	IGBT16	IGBT17	IGBT18
	53.8	52.9	60.1	59.2	59.9	59	58.8	58.4	59.5	58.4	54.1	53.2	55	53.5	60.7	59.4	60.5	59.2
IGBT	**IGBT19**	**IGBT20**	**IGBT21**	**IGBT22**	**IGBT23**	**IGBT24**	**IGBT25**	**IGBT26**	**IGBT27**	**IGBT28**	**IGBT29**	**IGBT30(**	**IGBT31**	**IGBT32**	**IGBT33**	**IGBT34**	**IGBT35**	**IGBT36**
	61.4	59.7	61.5	60	54.8	53.3	54	51.8	59.9	57.1	59.6	57	60.5	57.2	60.6	57.8	53.8	51.8

TABLE IV
SIMULATED SKIM909GD066 IGBTS MAXIMUM JUNCTION TEMPERATURES (IN °C) USING A WATER–GLYCOL SINGLE-PHASE COOLING SYSTEM WITH $T_{\text{in}} = 20$ °C, $P_d = 2106$ W (52 W/IGBT, 13 W/DIODE), AND DIFFERENT FLOW RATES

Flow rate	IGBT1	IGBT2	IGBT3	IGBT4	IGBT5	IGBT6	IGBT7	IGBT8	IGBT9	IGBT10	IGBT11	IGBT12	IGBT13	IGBT14	IGBT15	IGBT16	IGBT17	IGBT18
6 (l/min)	87.2	84.9	97.3	95.6	98.1	96.5	98.8	98.1	99.9	98.3	94.6	93.1	92.8	90.8	100.5	99.7	100.7	100.3
8 (l/min)	73.6	71.3	78.8	77.1	79.2	76.5	79.3	78	81	79.2	78.2	75.6	79	78.2	82.3	83.8	80.8	83.1
10 (l/min)	72.2	70.0	77.1	75.4	77.6	74.7	77.4	75.8	79.2	77.1	76.4	73.6	77.0	76.3	80.3	81.7	78.6	81.0
12 (l/min)	71.2	69.0	75.9	74.2	76.1	73.0	76.0	74.3	77.7	75.5	75.1	72.0	75.7	74.9	78.5	80.1	77.0	79.2
Flow rate	**IGBT19**	**IGBT20**	**IGBT21**	**IGBT22**	**IGBT23**	**IGBT24**	**IGBT25**	**IGBT26**	**IGBT27**	**IGBT28**	**IGBT29**	**IGBT30**	**IGBT31**	**IGBT32**	**IGBT33**	**IGBT34**	**IGBT35**	**IGBT36**
6 l/min	100.4	100.6	99.3	99.9	89.0	90.7	87.0	83.8	96.1	92.0	97.6	93.6	99.6	96.0	100.6	97.0	93.7	91.0
8 l/min	80.7	82.6	79.8	83	74.5	77.3	74.1	71.8	78.4	76.9	77.2	76.6	79.2	77.9	80.4	80	77.3	76.4
10 l/min	78.4	80.3	77.7	80.9	72.9	75.5	72.9	70.2	76.7	75.2	74.7	74.5	77.1	75.8	77.7	77.9	75.1	74.3
12 l/min	76.7	78.7	76.3	79.5	71.6	74.2	71.6	69.1	75.2	73.8	73.5	73.2	75.6	74.4	76.1	76.4	73.8	73.0

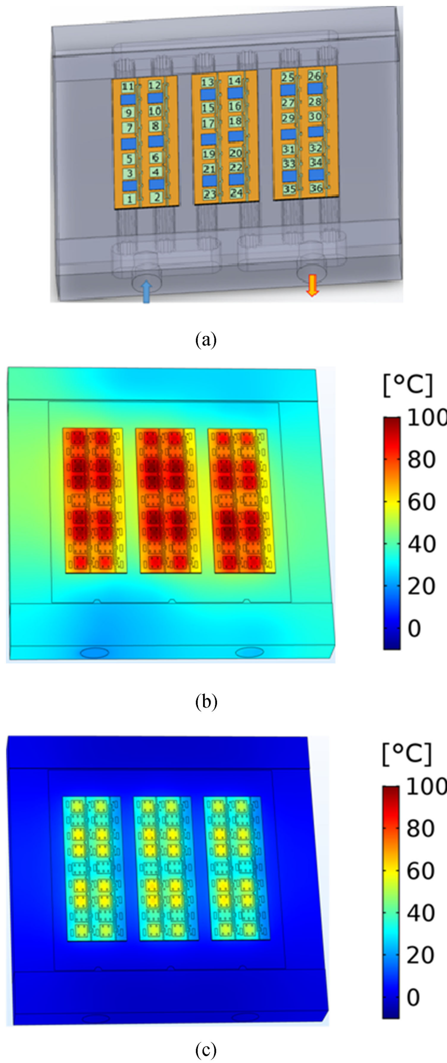

Fig. 9. Simulated temperature distribution at the silicon power device layer with $P_d = 2.1$ kW. (a) Diodes (in blue) and IGBTs (in green) layout inside the SKIM909GD066 power module, showing how were numbered the IGBTs. (b) Single-phase cooling with flow rate = 6 L/min and $T_{\text{in}} = 20$ °C. (c) Two-phase cooling with $T_{\text{sat}} = -8$ °C and flow rate = 0.2 L/min.

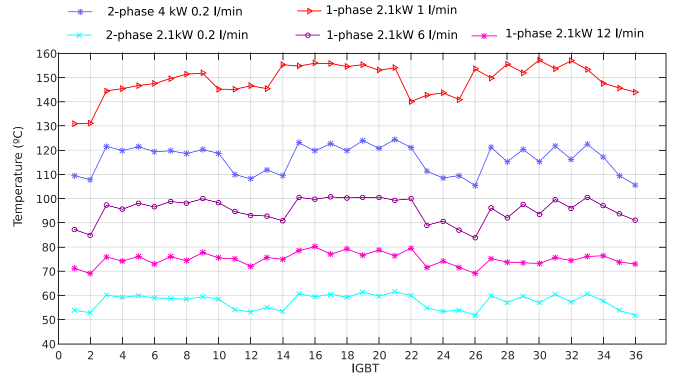

Fig. 10. SKIM909GD066 maximum IGBT simulated temperatures under the following operating conditions. 1) Single-phase cooling with $P_d = 2.1$ kW and $T_{\text{in}} = 20$ °C and different flow rates. 2) Two-phase cooling with Tsat = −8 °C and flow rate = 0.2 L/min, for total dissipated powers of 2.1 and 4 kW.

2106 W, with an R134a-cooled two-phase cold plate, the maximum IGBT temperature can be maintained below 62 °C, with $T_{\text{sat}} = -8$ °C and a flow rate of 0.2 L/min, whereas with a water single-phase cold plate, it would reach around 100 °C with a flow rate of 6 L/min and $T_{\text{in}} = 20$ °C. With low flow rates (less than 1 L/min as in the two-phase system), the IGBT temperature goes above its maximum allowable junction temperature (175 °C).

The maximum IGBT junction temperature as a function of the power module position is given in Fig. 10. It can be stated that two-phase cooling can achieve much lower IGBT temperatures than single-phase cooling, and moreover, two-phase cooling shows an almost constant heat exchange efficiency even at very low flow rates, where single-phase cooling becomes ineffective. The simulation of the single-phase technique with $P_d = 2.1$ kW, $T_{\text{in}} = 20$ °C, and flow rate = 1 L/min gives a $T_{\max} \cong 150$ °C and a temperature increase of the water close to 33 °C. Then, even if the maximum temperature of power devices is below the maximum allowed, the high temperature increase would imply to adopt an expensive chiller. With higher flow rates, 6 L/min or more, the temperature increase can be kept at the order of

magnitude of few degrees. For a closed-loop liquid cooling system, this allows the adoption of a simple radiator with fans to cool the water–glycol mixture at the desired temperature at the cold plate inlet.

For a dissipated power of 2106 W, single-phase cooling will produce a maximum gradient temperature of around 16 °C with a flow rate of 6 L/min and $T_{\text{inlet}} = 20$ °C among the IGBTs, while two-phase cooling can reduce it to around 10 °C, with $T_{\text{sat}} = -8$ °C and a flow rate of 0.2 L/min. Since the power conversion efficiency of the power electronic systems is determined also by the IGBT junction temperature and an uniform temperature among the IGBTs is highly desirable, it is obvious that two-phase cooling can improve the performance of the inverter from the point of view of both the conversion efficiency and the system reliability. A further comparison between single- and two-phase coolers can be done observing the results in Fig. 9, which shows the temperature distribution on the inverter module with water [see Fig. 9(c)] and R134-a [see Fig. 9(b)] as coolants. The large difference in the temperature values and distribution is due to the different physics governing these cooling solutions.

VI. Conclusion

A comparison of two-phase cooling with single-phase cooling has been done in order to address the advantages of the two-phase solution. In this way, a VCTPL technology has been demonstrated through a series of tests using a small-scale prototype. Then, a 3-D FEM-based thermal model has been designed to simulate two-phase cooling of IGBTs at the motor inverter.

The key conclusions of this study are the following.

1) Simulation of the complex two-phase phenomenon, with thermal transport by boiling and convection, can be simplified with a good matching between simulation and experimental results by the substitution of all the mechanisms by a simple uniform heat transfer coefficient, h, along the inner walls of the cold plate.
2) Simulation and experimental results show that two-phase cooling increases the heat transfer coefficient of a conventional cold plate.
3) For these h values, the two-phase FEM simulation shows that the maximum IGBT junction temperature can be maintained below 62 °C, whereas, with a water cooled system, it reaches 101 °C under same operation conditions.
4) FEM simulations show that the cooling capacity of the two-phase cooling system can be increased from 2.1 to 4 kW maintaining the IGBT junction temperature below 130 °C.
5) Two-phase cooling provides a more even temperature distribution among the IGBTs in the power module. For a dissipated power of 2106 W, single-phase cooling will produce a maximum gradient temperature of 16 °C among the IGBTs, while two-phase cooling can reduce it to 10 °C.
6) Two-phase cooling offers the possibility to run the module at higher current density and realizes the same power level with fewer devices and smaller/lighter weight packaging, resulting in significant potential cost savings.
7) When compared with competing cooling technologies based on passive two-phase cooling, such as flow boiling in microchannels, jet impingement, and spray cooling, this is the only one capable of lowering the junction temperature to values below the ambient temperature. A vapor compression two-phase thermal management system may be appropriate for designing power inverters used in applications where subambient temperatures are required.
8) The results of the experiments demonstrate that conventional automotive A/C system can be used for a more efficient cooling of power converters.

References

[1] A. Bhunia, S. Chandrasekaran, and C.-L. Chen, "Performance improvement of a power conversion module by liquid micro-jet impingement cooling," *IEEE Trans. Compon. Packag. Technol.*, vol. 30, no. 2, pp. 309–316, Jun. 2007.
[2] I. Mudawar, D. Bharathan, K. Kelly, and S. Narumanchi, "Two-phase spray cooling of hybrid vehicle electronics," in *Proc. Intersoc. Conf. Thermal Thermomech. Phenomena Electron. Syst.*, 2008, pp. 1210–1221.
[3] T. Kanata, K. Nishiwaki, and K. Hamada, "Development trends of power semiconductors for hybrid vehicles," in *Proc. Int. Power Electron. Conf.*, 2010, pp. 778–782.
[4] A. Bar-Cohen and J. J. Albrecht, J. D. and Maurer, "Near-junction thermal management for wide bandgap devices," in *Proc. IEEE Compound Semicond. Integr. Circuit Symp.*, Oct. 2011, pp. 1–5.
[5] S. Anandan and V. Ramalingam, "Thermal management of electronics: A review of literature," *Therm. Sci.*, vol. 12, p. 26, 2008.
[6] U. M. Choi, F. Blaabjerg, and K. B. Lee, "Study and handling methods of power IGBT module failures in power electronic converter systems," *IEEE Trans. Power Electron.*, vol. 30, no. 5, pp. 2517–2533, May 2015.
[7] R. Amro, J. Lutz, and A. Lindemann, "Power cycling with high temperature swing of discrete components based on different technologies," in *Proc. IEEE 35th Annu. Power Electron. Spec. Conf.*, 2004, vol. 4, pp. 2593–2598.
[8] L. Meysenc, M. Jylhakallio, and P. Barbosa, "Power electronics cooling effectiveness versus thermal inertia," *IEEE Trans. Power Electron.*, vol. 20, no. 3, pp. 687–693, May 2005.
[9] A. Bar-Cohen, R. Bahadur, and M. Iyengar, "Least-energy optimization of air-cooled heat sinks for sustainability—Theory, geometry and material selection," *Energy*, vol. 31, pp. 579–619, 2006.
[10] P. Rodgers and V. Eveloy, "Air cooled heat sink design optimization in free convection," in *Proc. Semicond. Thermal Meas. Manag. Symp.*, 2013, pp. 170–172.
[11] A. Wintrich, U. Nicolai, W. Tursky, and T. Reimann, *Application Manual Power Semiconductor*. Nuremberg, Germany: Semikron Int. GmbH, 2011.
[12] S. Kang, "Advanced cooling for power electronics," in *Proc. Int. Conf. Integr. Power Electron. Syst.*, 2012, pp. 1–8.
[13] J. Schulz-Harder, K. Exel, and A. Meyer, "Direct liquid cooling of power electronics devices," in *Proc. Int. Conf. Integr. Power Electron. Syst.*, 2006, pp. 1–6.
[14] D. Saums, "Applications of vaporizable dielectric fluid cooling for IGBT power semiconductors," in *Proc. Semicond. Thermal Meas. Manag. Symp.*, 2011, pp. 253–264.
[15] N. Jankowski, L. Everhart, B. Morgan, B. Geil, and P. McCluskey, "Comparing microchannel technologies to minimize the thermal stack and improve thermal performance in hybrid electric vehicles," in *Proc. Veh. Power Propulsion Conf.*, 2007, pp. 124–130.
[16] J. Marcinkowski, "Dual-sided cooling of power semiconductor modules," in *Proc. Int. Exhib. Conf. Power Electron., Intell. Motion, Renew. Energy Energy Manage.*, 2014, pp. 1–7.
[17] R. C. Burns, "Vertical integration power modules for double sided cooling applications using aluminum conductors and thick film dielectrics," in *Proc. Int. Exhib. Conf. Power Electron., Intell. Motion, Renew. Energy Energy Manage.*, 2014, pp. 1–8.
[18] C. Buttay *et al.*, "High performance cooling system for automotive inverters," in *Proc. Eur. Conf. Power Electron. Appl.*, 2007, pp. 1–9.

[19] M. Schneider-Ramelow, T. Baumann, and E. Hoene, "Design and assembly of power semiconductors with double-sided water cooling," in *Proc. Int. Conf. Integr. Power Electron. Syst.*, 2008, pp. 1–7.

[20] C. Gobl and J. Faltenbacher, "Low temperature sinter technology die attachment for power electronic applications," in *Proc. Int. Conf. Integr. Power Electron. Syst.*, 2010, pp. 1–5.

[21] J. Kim, "Spray cooling heat transfer: The state of the art," *Int. J. Heat Fluid Flow*, vol. 28, pp. 753–767, 2007.

[22] H. Bostanci, D. Van Ee, B. Saarloos, D. Rini, and L. Chow, "Thermal management of power inverter modules at high fluxes via two-phase spray cooling," *IEEE Trans. Compon. Packag. Manuf. Technol.*, , vol. 2, no. 9, pp. 1480–1485, Sep. 2012.

[23] D. Bharathan and V. Hassani, "Spray cooling: An assessment for use with automotive power electronics applications," Nat. Renew. Energy Lab., Golden, CO, USA, Milestone Rep. FY05-7000, 2005.

[24] L. Turek, D. Rini, B. Saarloos, and L. Chow, "Evaporative spray cooling of power electronics using high temperature coolant," in *Proc. Intersoc. Conf. Thermal Thermomech. Phenomena Electron. Syst.*, 2008, pp. 346–351.

[25] R. G. Mertens *et al.*, "Spray cooling of IGBT devices," *J. Electron. Packag.*, vol. 129, pp. 316–323, 2007.

[26] K. Olesen, F. Osterwald, M. Tonnes, R. Drabek, and R. Eisele, "Direct liquid cooling of power modules in converters for the wind industry," in *Proc. Int. Exhib. Conf. Power Electron., Intell. Motion, Renew. Energy Energy Manage.*, 2010, pp. 742–747.

[27] A. Bhunia and C.-L. Chen, "Jet impingement cooling of an inverter module in the harsh environment of a hybrid vehicle," *Heat Transfer Div. Electron. Photon. Packag. Div.*, vol. 4, pp. 561–567, 2005.

[28] K. Gould, S. Cai, C. Neft, and A. Bhunia, "Liquid jet impingement cooling of a silicon carbide power conversion module for vehicle applications," *IEEE Trans. Power Electron.*, vol. 30, no. 6, pp. 2975–2984, Jun. 2015.

[29] P. R. Parida, S. V. Ekkad, and K. Ngo, "Impingement-based high performance cooling configurations for automotive power converters," *Int. J. Heat Mass Transfer*, vol. 55, pp. 834–847, 2012.

[30] K. Kellly, T. Abrahan, K. Bennion, D. Bharathan, S. Narumanchi, and M. O'Keefe, "Assessment of thermal control technologies for cooling electric vehicle power electronics," in *Proc. Int. Electr. Veh. Symp.*, 2007.

[31] C. Barnes and P. Tuma, "Practical considerations relating to immersion cooling of power electronics in traction systems," *IEEE Trans. Power Electron.*, vol. 25, no. 9, pp. 2478–2485, Sep. 2010.

[32] E. Laloya, Ó. Lucía, H. Sarnago, and J. M. Burdío, "Heat management in power converters: From state of the art to future ultrahigh efficiency systems," *IEEE Trans. Power Electron.*, vol. 31, no. 11, pp. 7896–7908, Nov. 2016.

[33] I. Mudawar, "Assessment of high-heat-flux thermal management schemes," *IEEE Trans. Compon. Packag. Technol.*, vol. 24, no. 2, pp. 122–141, Jun 2001.

[34] H. Bostanci, D. V. Ee, B. A. Saarloos, D. P. Rini, and L. C. Chow, "Thermal management of power inverter modules at high fluxes via two-phase spray cooling," *IEEE Trans. Compon. Packag. Manuf. Technol.*, vol. 2, no. 9, pp. 1480–1485, Sep. 2012.

[35] M. Lee and J. Issam, "Two-phase flow in high-heat-flux micro-channel heat sink for refrigeration cooling applications: Part II—Heat transfer characteristics," *Int. J. Heat Mass Transfer*, vol. 48, pp. 941–955, 2005.

[36] M. Lee and J. Issam, "Two-phase flow in high-heat-flux micro-channel heat sink for refrigeration cooling applications: Part I—Pressure drop characteristics," *Int. J. Heat Mass Transfer*, vol. 48, pp. 928–940, 2005.

[37] J. Lee and I. Mudawar, "Low-temperature two-phase micro-channel cooling for high-heat-flux thermal management of defense electronics," in *Proc. Intersoc. Conf. Thermal Thermomech. Phenomena Electron. Syst.*, 2008, pp. 132–144.

[38] N. Malu, D. Bora, S. Nakanekar, and S. Tonapi, "Thermal management of an IGBT module using two-phase cooling," in *Proc. Intersoc. Conf. Thermal Thermomech. Phenomena Electron. Syst.*, 2014, pp. 1079–1085.

[39] J. Campbell, L. Tolbert, C. Ayers, B. Ozpineci, and K. Lowe, "Two-phase cooling method using the R134a refrigerant to cool power electronic devices," *IEEE Trans. Ind. Appl.*, vol. 43, no. 3, pp. 648–656, May/Jun. 2007.

[40] K. Lowe, C. Avers, and J. Hsu, "Operating controls and dynamics for floating refrigerant loop for high heat flux electronics," in *Proc. Semicond. Thermal Meas. Manage. Symp.*, 2006, pp. 126–129.

[41] G. Moreno, J. Jeffers, S. Narumanchi, and K. Bennion, "Passive two-phase cooling of automotive power electronics," in *Proc. Semicond. Thermal Meas. Manage. Symp.*, 2014, pp. 58–65.

[42] P. Wang, P. McCluskey, and A. Bar-Cohen, "Two-phase liquid cooling for thermal management of IGBT power electronic module," *J. Electron. Packag.*, vol. 135, 2013, Art. no. 021001.

[43] A. Cavallini, G. Censi, D. D. Col, L. Doretti, G. Longo, and L. Rossetto, "Experimental investigation on condensation heat transfer and pressure drop of new HFC refrigerants (R134a, R125, R32, R410A, R236ea) in a horizontal smooth tube," *Int. J. Refrigeration*, vol. 24, pp. 73–87, 2001.

[44] S. M. R., "Potential refrigerants for power electronics cooling," Oak Ridge Nat. Lab., Oak Ridge, TN, USA, Tech. Rep. ORNL/TM-2005/219, 2005.

[45] M. Lazzaroni *et al.*, "Metrological characterization of cold plates for power converters," *IEEE Trans. Instrum. Meas.*, vol. 65, no. 1, pp. 37–45, Jan. 2016.

[46] Y. Madhour, J. Olivier, E. Costa-Patry, S. Paredes, B. Michel, and J. Thome, "Flow boiling of R134a in a multi-microchannel heat sink with hotspot heaters for energy-efficient microelectronic CPU cooling applications," *IEEE Trans. Compon. Packag. Manuf. Technol.*, vol. 1, no. 6, pp. 873–883, Jun. 2011.

[47] C. Park and E. Sunada, "Vapor compression hybrid two-phase loop technology for lunar surfaces applications," in *Proc. AIP Conf.*, 2009, p. 969.

[48] L. Yu and D. Liu, "Study of the thermal effectiveness of laminar forced convection of nanofluids for liquid cooling applications," *IEEE Trans. Compon. Packag. Manuf. Technol.*, vol. 3, no. 10, pp. 1693–1704, Oct. 2013.

[49] H. Lee, L. Song, H. Yunho, R. Reinhard, and C. Ho-Hwan , "Experimental investigations on flow boiling heat transfer in plate heat exchanger at low mass flux condition," *Appl. Thermal Eng.*, vol. 61, no. 2, pp. 408–415, 2013.

[50] M. A. H. Rasid, A. Ospina, K. E. K. Benkara, and V. Lanfranchi, "A thermal study on small synchronous reluctance machine in automotive cycle," in *Proc. IEEE 25th Int. Symp. Ind. Electron.*, 2016, pp. 134–140.

[51] S. F. Tie and C. W. Tan, "A review of energy sources and energy management system in electric vehicles," *Renew. Sustain. Energy Rev.*, vol. 20, pp. 82–102, 2013.

[52] P. Beckedahl, T. Grasshoff, and M. Lederer, "A new power module concept for automotive applications," in *Proc. Int. Exhib. Conf. Power Electron., Intell. Motion, Renew. Energy Energy Manage.*, 2007.

Itxaso Aranzabal received the B.Sc. degree in industrial electronic engineering from the University of Deusto, Bilbao, Spain, in 2003, and the M.Sc. degree in automatization and industrial electronic engineering from the University of Deusto, Bilbao, in 2010. She is currently working toward the Ph.D. degree with the University of the Basque Country, Bilbao.

Her current research interests include high-power insulated-gate bipolar transistor module reliability and modeling.

Iñigo Martínez de Alegría received the B.Sc. and M.Sc. degrees in physics and the Ph.D. degree from the University of the Basque Country, Bilbao, Spain, in 1996 and 2012, respectively.

For two years, he was with Ikerlan, a research center of the MCC Industrial Group in mechatronics applications. Then, he was with Azterlan, a metallurgy research center. Since 2000, he has been an Associate Professor with the University of the Basque Country. His current research interests include application of power electronics to renewable energies.

Nicola Delmonte (M'15) was born in Manfredonia, Italy, in 1967. He received the Laurea degree in electronic engineering and the Ph.D. degree in information technology from the University of Parma, Parma, Italy, in 2002 and 2006, respectively.

Since 2002, he has been with the Department of Engineering and Architecture (formerly Information Engineering), University of Parma, where he became a Research Fellow in 2005, an Assistant Professor in 2013, and an Associate Professor in 2018. His research activities have covered the study of breakdown phenomena and high-field accelerated stress of pseudomorphic high-electron-mobility transistors, the technological processing for radio frequency test structures on thin ceramic films, the electrical and thermal characterization, modeling, and reliability evaluation of power devices and hybrid modules, the design of renewable-energy plants, nanogrids, and smart systems.

Dr. Delmonte was the second place winner of the International Competition of Ideas entitled "Renewable energy for the smaller islands and marine protected areas" (Issue 2011), promoted by the Environmental Association Marevivo and the Italian Ministry of Environment and Protection of Territory and Sea.

Paolo Cova was born in Milan, Italy, in 1966. He received the M.S. degree in electronic engineering and the Ph.D. degree in information technology from the University of Parma, Parma, Italy, in 1992 and 1996, respectively.

He is currently a Professor with the University of Parma. He worked on characterization and reliability evaluation of electronic and optoelectronic III–V compound semiconductor devices, thermal modeling, and reliability of power devices and converters. He has authored more than 130 scientific papers in international journals or international conference proceedings in these fields. He collaborates with the Istituto Nazionale di Fisica Nucleare on thermal studies of power electronics for the ATLAS Experiment at the European Organization for Nuclear Research. He has been involved in teaching with the School of Engineering, University of Parma, since 1995. At present, he is teaching industrial electronics at the electronics engineering master course. Since 2011, he has been an ERASMUS delegate for the Department of Engineering and Architecture, University of Parma.

Dr. Cova is a reviewer for international journals (including some IEEE Transactions). He was the Technical Program Committee Chair of the European Conference on Reliability of Electron Devices (ESREF) and a Guest Editor for *Microelectronics Reliability*. He was a twice recipient of the Best Paper Award at the ESREF.

Iñigo Kortabarria received the M.Sc. degree in electronic and control engineering from the University of Mondragon, Mondragon, Spain, in 1999, and the Ph.D. degree from the University of the Basque Country, Bilbao, Spain, in 2013.

From 1999 to 2004, he was an R&D Staff Member in industrial electronics companies. From 2004 to 2014, he was an Assistant Professor in electronic technology with the Electronics Technology Department, University of the Basque Country, where he became an Associate Professor in 2014. His current research interests include control of power converter topologies for electric vehicles.